Volume 14
Number 7
July 2023
Pages 1201–1390

RSC Medicinal Chemistry

rsc.li/medchem

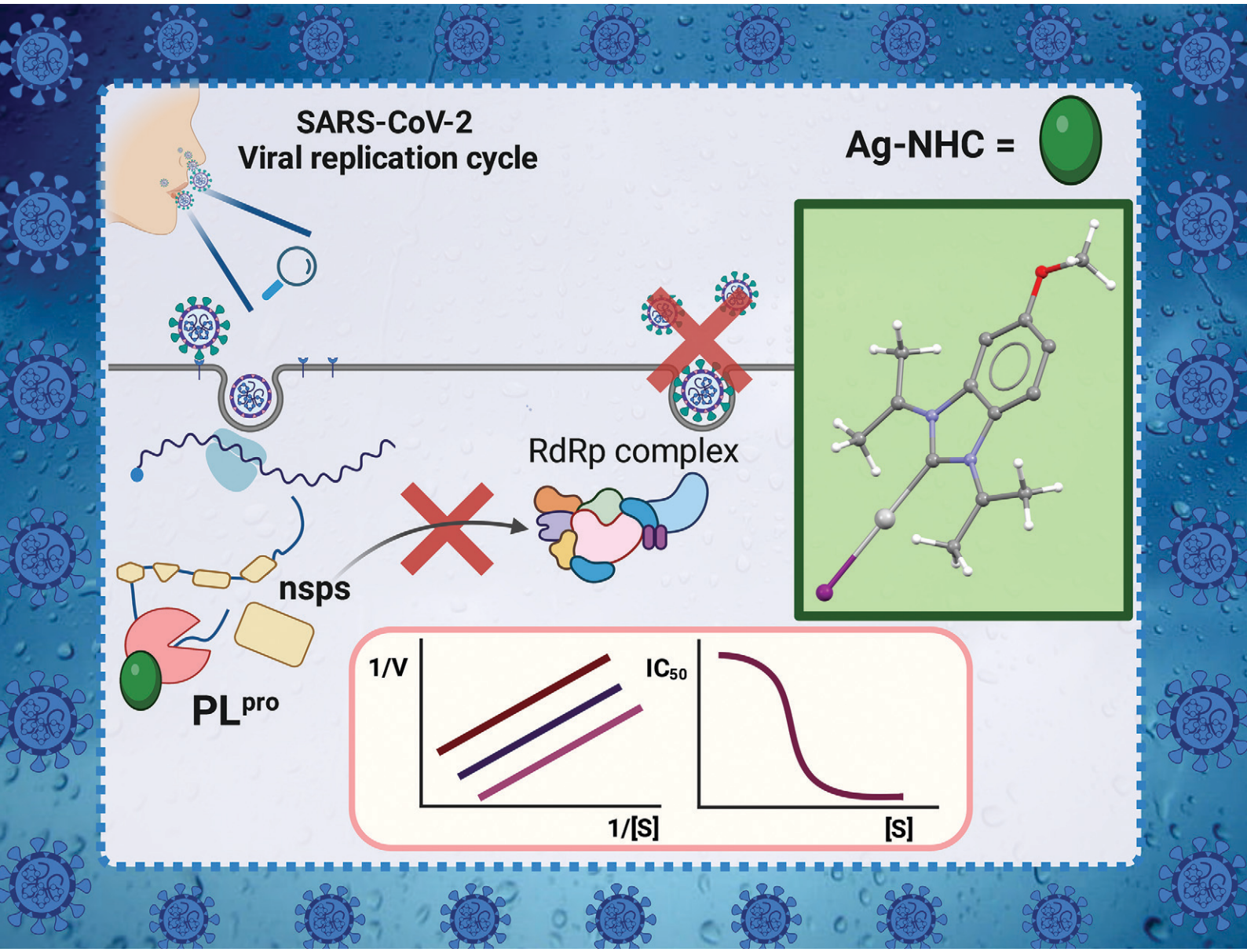

ISSN 2632-8682

ROYAL SOCIETY OF CHEMISTRY

RESEARCH ARTICLE
Ingo Ott *et al.*
Silver N-heterocyclic carbene complexes are potent uncompetitive inhibitors of the papain-like protease with antiviral activity against SARS-CoV-2

RSC Medicinal Chemistry

ROYAL SOCIETY OF CHEMISTRY

RESEARCH ARTICLE

View Article Online
View Journal | View Issue

Cite this: *RSC Med. Chem.*, 2023, **14**, 1260

Silver N-heterocyclic carbene complexes are potent uncompetitive inhibitors of the papain-like protease with antiviral activity against SARS-CoV-2†

Maria Gil-Moles,[ab] Cillian O'Beirne,[a] Igor V. Esarev,[a] Petra Lippmann,[a] Matthias Tacke,[c] Jindrich Cinatl Jr.,[d] Denisa Bojkova[d] and Ingo Ott *[a]

Received 10th February 2023,
Accepted 3rd May 2023

DOI: 10.1039/d3md00067b

rsc.li/medchem

The ongoing SARS-CoV-2 pandemic has caused a high demand for novel innovative antiviral drug candidates. Despite promising results, metal complexes have been relatively unexplored as antiviral agents in general and in particular against SARS-CoV-2. Here we report on silver NHC complexes with chloride or iodide counter ligands that are potent inhibitors of the SARS-CoV-2 papain-like protease (PL^{pro}) but inactive against 3C-like protease ($3CL^{pro}$) as another SARS-CoV-2 protease. Mechanistic studies on a selected complex confirmed zinc removal from a zinc binding domain of PL^{pro} as relevant factor of their activity. In addition, enzyme kinetic experiments revealed that the complex is an uncompetitive inhibitor and with this rare type of inhibition it offers great pharmacological advantages in terms selectivity. The silver NHC complexes with iodide ligands showed very low or absent host cell toxicity and triggered strong effects on viral replication in cells infected with SARS-CoV-2, making them promising future antiviral drug candidates.

Introduction

Since the discovery of the antitumoral properties of the platinum complex cisplatin, which has become the iconic lead compound for metallodrugs in general, there have been increasing efforts and many success stories regarding the development of metal-based cytostatics.[1,2] Among few other therapeutic indications, infectious diseases have emerged as an additional relevant therapeutic field for new metallodrug candidates, with antibacterial agents as the most intensively studied class.[2,3]

Due to the ongoing SARS-CoV-2 pandemic, the spotlight has been shifted towards viral infections, an area that has been relatively underexplored regarding metal-based bioactive substances.[4–6] However, a slowly increasing number of reports on metal complexes with activity in SARS-CoV-2 infection models confirms the potential of metal complexes in this area.[7–10]

We have recently reported on gold and other metal complexes as inhibitors of the SARS-CoV-2 papain-like protease PL^{pro} and the interaction of the viral spike protein with the host cell ACE2 receptor.[8,11] In particular for the cysteine protease PL^{pro}, which is essential for viral replication in infected cells, very promising enzyme inhibitory activity has been observed with various metal complexes and the triggering of antiviral effects against SARS-CoV-2 has been confirmed in infected cells. Among the promising hit compounds were some silver complexes, of which an example with a N-heterocyclic carbene (NHC) ligand displayed very promising activity as a PL^{pro} inhibitor and antiviral agent against SARS-CoV-2 (see Fig. 1).[8] Inhibitors of PL^{pro} have recently attracted increasing attention in SARS-CoV-2 drug discovery projects.[12]

The anti-infective properties of silver NHC complexes have been well studied going back to a first report by Youngs *et al.* in 2004 on antibacterial activity.[13] To date, many reports

[a] *Institute of Medicinal and Pharmaceutical Chemistry, Technische Universität Braunschweig, Beethovenstr. 55, 38106 Braunschweig, Germany. E-mail: ingo.ott@tu-bs.de*
[b] *Departamento de Química, Universidad de La Rioja, Centro de Investigación de Síntesis Química (CISQ), Complejo Científico Tecnológico, 26004 Logroño, Spain*
[c] *School of Chemistry, University College Dublin, Belfield, Dublin 4, Ireland*
[d] *Institute of Medical Virology, Universitätsklinikum Frankfurt, Paul-Ehrlich-Str. 40, 60596 Frankfurt, Germany*

† Electronic supplementary information (ESI) available. See DOI: https://doi.org/10.1039/d3md00067b

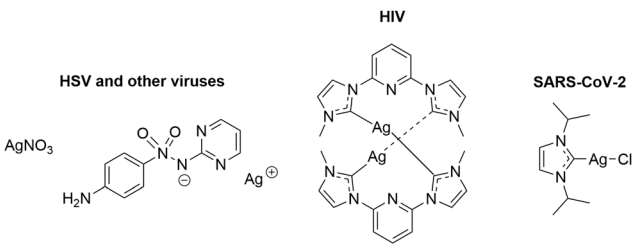

Fig. 1 Previously reported antiviral silver complexes.[4,8,16]

provide strong evidence on the antibacterial properties of silver NHC complexes (*e.g.* complex SBC3) and their efficacy has been proven both *in vitro* and *in vivo*.[14,15]

As for the antiviral activity of silver complexes, the number of reports is comparably limited, despite that silver nitrate and other silver compounds showed efficacy against herpes simplex and other viruses.[4] Interestingly, a macrocyclic silver complex with a NHC ligand displayed strong antiviral activity against HIV-1.[16]

Based on the above screening results, we have extended our studies on silver NHC complexes as possible antiviral agents against SARS-CoV-2. A series of complexes, including the antibacterial SBC3 as reference, was prepared, characterized and evaluated as inhibitors of the target enzymes PL^{pro} and $3CL^{pro}$. Non-toxic examples were selected for antiviral studies in SARS-CoV-2 infected cells. The results of this study are presented in this paper.

Chemistry

The target silver NHC complexes could be obtained by an established procedure (see Scheme 1) going back to the method reported by Wang and Lin in 1998.[17] In the first step, the respective (benz)imidazoles were alkylated leading to the respective (benz)imidazolium iodides **1**–**4**. To obtain the silver NHC chlorido complexes **Ag-1a**–**Ag-4a**, the iodide counterion of **1**–**4** was replaced with chloride followed by treatment with silver oxide. The silver NHC iodido complexes **Ag-1b**–**Ag-4b** could be generated directly from **1**–**4** by reaction with silver oxide. All silver NHC complexes could be prepared in high purity as evidenced by elemental analysis measurements (maximum deviation of the theoretical values: ≤0.5%).

The disappearance of the hydrogen signal at position 2 of the (benz)imidazolium cations at 10.72–11.86 ppm in the ^{1}H-NMR spectra of the silver NHC complexes **Ag-1a**/**b**–**Ag-4a**/**b** is a clear confirmation of formation of the metal carbon bond. Comparing the ^{13}C-NMR spectra of the chlorido complexes **Ag-1a** to **Ag-4a** with those of the respective iodido analogues **Ag-1b** to **Ag-4b**, shows that the C2 signals of the chlorido complexes are shifted approx. 2–3 ppm towards the upper field compared with the analogous iodido complexes (see ESI† Fig. S1). An increase in the σ-donor ability or, in other words, a lower electronegativity of the halogene ligand should cause a decrease in the Lewis acidity of the metal, which results in the observed increasing ^{13}C chemical shift of C2.[18]

Mass spectrometry (ESI) measurements showed biscarbene formation with the respective [M–X + NHC] signals in the positive and the AgX_2^- counterions in the negative mode.

In solution silver NHC complexes exist in a dynamic equilibrium between the neutral monomeric [(NHC)AgX] form and a cationic dimeric $[(NHC)_2Ag]^+$ form with a AgX_2^- counter ion (see Fig. 2).[17,19–21] In the solid state various bonding motifs can exist, while in solution also the monomeric form can be dominant. The lack of a ^{13}C–^{107,109}Ag coupling in the ^{13}C-NMR spectra of complexes **Ag-1a**/**b**–**Ag-4a**/**b** is indicative of such fluxional behaviour with a fast equilibrium in solution indicating dominance of the monomeric form.[17,21] In addition, ^{109}Ag-NMR spectra taken exemplarily for complexes **Ag-4a**/**b** show a single narrow signal, also indicative of a predominant and likely monocarbenic form. The observed chemical shift for **Ag-4a** is 633.6 ppm. There is only one example of ^{109}Ag-NMR of a monomeric [(NHC)AgCl] complex in the literature, where the signal was detected at 597 ppm.[22] An additional and even more interesting aspect is the difference in the chemical shifts observed for **Ag-4a** (chloride) and **Ag-4b** (iodide). Compared with **Ag-4a**, the signal for compound **Ag-4b** is strongly shifted towards low field and it appears at 709.7 ppm. To the best of our knowledge, this is the first report of a ^{109}Ag-NMR signal for a [(NHC)AgI] complex. Although, in the literature there are some examples of ^{109}Ag-NMR for silver biscarbenes, $[(NHC)_2Ag]^+$, where the signals appear at 642 ppm (ref. 23) and at 727 ppm,[24] the latter for a complex with ferrocenyl side chains. The data obtained with both ^{13}C-NMR and ^{109}Ag-NMR overall confirm significant differences in the electronic environments of the silver ions in [(NHC)AgCl] *vs.* [(NHC)AgI] complexes.

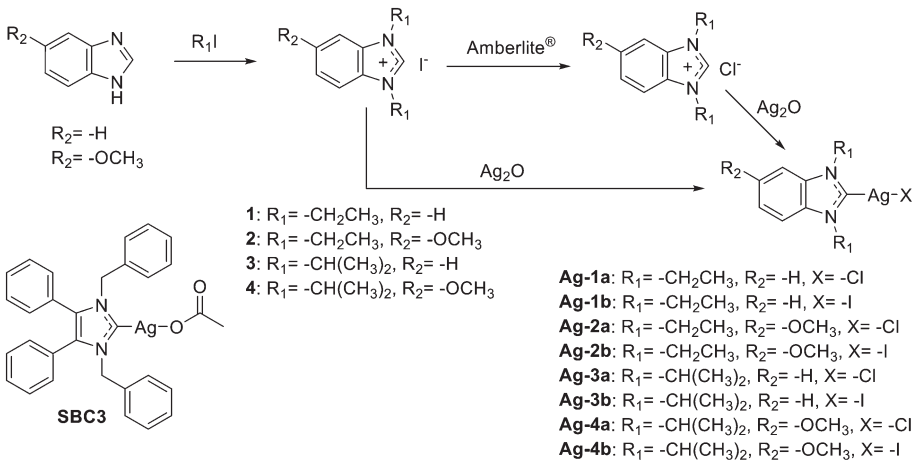

Scheme 1 Synthesis of silver(I) NHC complexes and structure of SBC3.

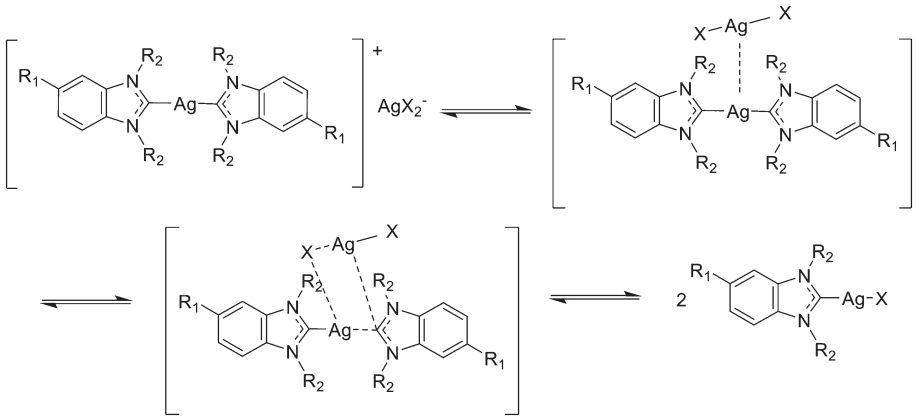

Fig. 2 Fluxional behaviour of silver(I) NHC complexes.

Conductivity measurements can be used to further distinguish between neutral and charged complexes in solution. Here we measured the conductivity of the silver NHC complexes in DMSO in comparison to the 1 : 1 electrolyte $AgNO_3$ after different periods up to 48 h (see Table 1). All silver NHC complexes generally showed much lower conductivity than $AgNO_3$ (S mol^{-1} cm^2 values of 2.15 to 9.70 for the silver NHC complexes *vs.* 38 for $AgNO_3$), which again supports that the organometallics exist predominantly in the neutral monocarbene form in DMSO solution. The values remained very stable over 48 h with only marginal increases in some cases, confirming that the equilibrium was formed immediately after dissolution and remained unaltered over the course of the experiment.

Complexes **Ag-3a** (chlorido), **Ag-3b** (iodido) and SBC3 (acetato) were selected as examples with different secondary ligands for conductometry experiments in diluted solutions (see ESI† Fig. S2). In these experiments the molecular conductivity values of **Ag-3b** only slightly increased upon decreasing the concentrations. In contrast, the values for **Ag-3a** and SBC3 showed roughly a 2–4 fold increase upon 10-fold dilution, indicating that for the complexes with chloride or acetate ligands the contribution of the charged (biscarbene) form could be increased at lower concentrations.

Enzymatic inhibition studies with SARS-CoV-2 PL^{pro} and $3CL^{pro}$

The inhibition of SARS-CoV-2 PL^{pro} and $3CL^{pro}$ as two relevant SARS-CoV-2 proteases was studied by enzymatic FRET assays and IC_{50} values were determined for the active inhibitors (see Table 2). Complexes **Ag-1a**/**b**–**Ag-4a**/**b**, SBC3 and silver nitrate were evaluated in concentrations up to 50 μM. Disulfiram (PL^{pro}) and GC376 ($3CL^{pro}$) served as positive reference inhibitors of the enzymes.

Against $3CL^{pro}$, none of the silver complexes reached more than 50% enzyme inhibition at the highest applied dosage of 50 μM. At this comparably high concentration only SBC3 showed some moderate inhibition of the enzymatic activity, while all other silver NHC complexes were completely inactive.

All silver NHC complexes were potent inhibitors of SARS-CoV-2 PL^{pro} with IC_{50} values in a rather narrow range of 0.2–0.4 μM, which is in excellent agreement with the results obtained with the silver NHC complex of our previous report.[8] Whereas structure–activity-relationships regarding the NHC or the halide ligands could not be identified, it should be noted that all silver NHC complexes exceeded the activity of the reference compounds silver nitrate and disulfiram as SARS-CoV-2 PL^{pro} inhibitors.

Table 1 Conductivity Λ_M, S mol^{-1} cm^2 for 1.0 mM solutions in DMSO

	Start	24 h	48 h
$AgNO_3$	38	38	38
SBC3	2.15	2.25	2.31
Ag-1a	3.00	3.09	3.31
Ag-1b	8.44	9.31	9.70
Ag-2a	2.94	3.13	3.37
Ag-2b	9.19	9.25	9.82
Ag-3a	2.34	2.70	2.67
Ag-3b	6.67	7.00	6.69
Ag-4a	2.15	2.25	2.40
Ag-4b	6.72	6.92	7.32

Table 2 Inhibition of $3CL^{pro}$ and PL^{pro} activity by the test compounds. IC_{50} values (μM) are presented as mean values ± standard deviation of 2 independent experiments. ">50" indicates that no IC_{50} could be calculated. The values between brackets represent the percentage of activity of the enzyme in presence of 50 μM of the test compound ± standard deviation of 2 independent experiments; n.d.: not determined

	$3CL^{pro}$ (SARS-CoV-2)	PL^{pro} (SARS-CoV-2)	PL^{pro} (SARS-CoV)
Disulfiram	n.d.	1.05 ± 0.31	5.52 ± 0.10
GC376	0.90 ± 0.20	n.d.	n.d.
4	n.d.	105 ± 2	103 ± 2
$AgNO_3$	>50 (97 ± 6%)	0.70 ± 0.27	12.05 ± 0.87
SBC3	>50 (70 ± 4%)	0.26 ± 0.03	n.d.
Ag-1a	>50 (106 ± 2%)	0.21 ± 0.03	n.d.
Ag-1b	>50 (110 ± 0%)	0.24 ± 0.11	n.d.
Ag-2a	>50 (98 ± 15%)	0.18 ± 0.02	n.d.
Ag-2b	>50 (115 ± 4%)	0.43 ± 0.06	n.d.
Ag-3a	>50 (116 ± 5)	0.21 ± 0.02	n.d.
Ag-3b	>50 (111 ± 14%)	0.19 ± 0.04	n.d.
Ag-4a	>50 (115 ± 4%)	0.22 ± 0.11	n.d.
Ag-4b	>50 (116 ± 2%)	0.39 ± 0.07	13.71 ± 1.02

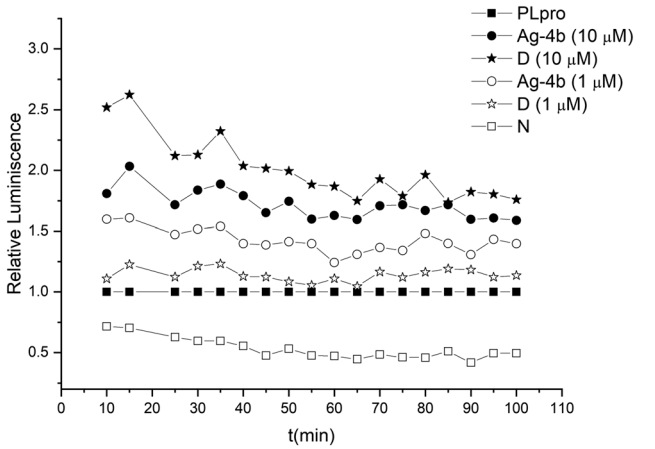

Fig. 3 Zn ejection from 0.5 μM SARS-CoV-2 PL^{pro} by 1.0 and 10.0 μM of test compounds. The relative luminescence compared with the untreated control was measured over 100 min. D: disulfiram; N: negative control (solvent).

Complex **Ag-4b** was selected for additional mechanistic studies on the nature of the inhibition of PL^{pro}. Initially, the related metal free (benz)imidazolium iodide **4** was exemplarily tested as reference and was inactive (IC_{50} value >100 μM), which confirmed that the silver ions are essential for enzymatic inhibition. Next, complex **Ag-4b** was studied as inhibitor of SARS-CoV PL^{pro} and showed an IC_{50} value of 13.71 μM. Taken together with the inactivity against $3CL^{pro}$, it can be concluded that the silver NHC complexes are selective inhibitors of PL^{pro} from SARS-CoV-2.

Time dependent studies on the inhibition of SARS-CoV-2 PL^{pro} by **Ag-4b** were done at a fixed concentration of 0.75 μM (see Fig. S3†) and showed that the enzymatic turnover was reduced to approx. 60% of the untreated control immediately at the beginning of the experiment up to 30 min of exposure. After 60 min the activity was decreased to approx. 40%. These data clearly indicate that the enzymatic inhibition occurs immediately with some increase over extended exposure.

SARS-CoV-2 PL^{pro} harbours a zinc binding domain that is responsible for the structural integrity of the enzyme and where the metal is coordinated by cysteine residues.[25] In our previous paper we had reported on the Zn ejection from PL^{pro} by gold complexes using an assay that detects free Zn ions with a fluorescent sensor molecule.[11,26] As Zn replacement from cysteines is also feasible for the soft Lewis acidic silver compounds, we investigated complex **Ag-4b** for Zn ejection properties in the same assay with the Zn-ejector disulfiram as a reference (see Fig. 3). In fact, the complex was effective in removing Zn from SARS-CoV-2 PL^{pro} with a similar efficacy as disulfiram (low efficacy at 1.0 μM and high efficacy at 10 μM).

An enzyme kinetic analysis was performed exemplarily for **Ag-4b**. With K_m values between 411 and 176 μM (for **Ag-4b** = 0, 0.1, 0.25, 0.75 μM, respectively) that are much higher than the K_i value (0.48 ± 0.22 μM), as well as the parallel lines in the Lineweaver–Burk representation (see Fig. 4, left), a clear pattern of an uncompetitive enzyme inhibitor was obtained. As such **Ag-4b** interacts only with the enzyme-substrate complex, but not with the enzyme alone.[27] Accordingly, increasing substrate concentrations will lead to a "paradox" decrease of IC_{50} values. This was further evaluated for **Ag-4b** and in fact the IC_{50} values at low substrate levels were much higher than those at high levels (see Fig. 4, right). A more detailed analysis of the Michaelis–Menten enzyme kinetics of **Ag-4b** is presented in the ESI.†

Cytotoxicity evaluation against CaCo-2 cell layers

Toxicity of test compounds against host cells can lead to false positive results in cell-based antiviral assays. In order to exclude toxic compounds and to evaluate in which concentration range the complexes could be applied in subsequent antiviral assays, almost confluent cell layers of CaCo-2 cells were grown and challenged for 24 h or 48 h with the complexes in concentrations between 25 μM and 500 μM. Fig. 5 exemplarily shows the effect of 100 μM of the test compounds against Caco-2 cells. At this concentration the iodido silver NHC complexes **Ag-1b** to **Ag-4b** are not cytotoxic, whereas all other complexes

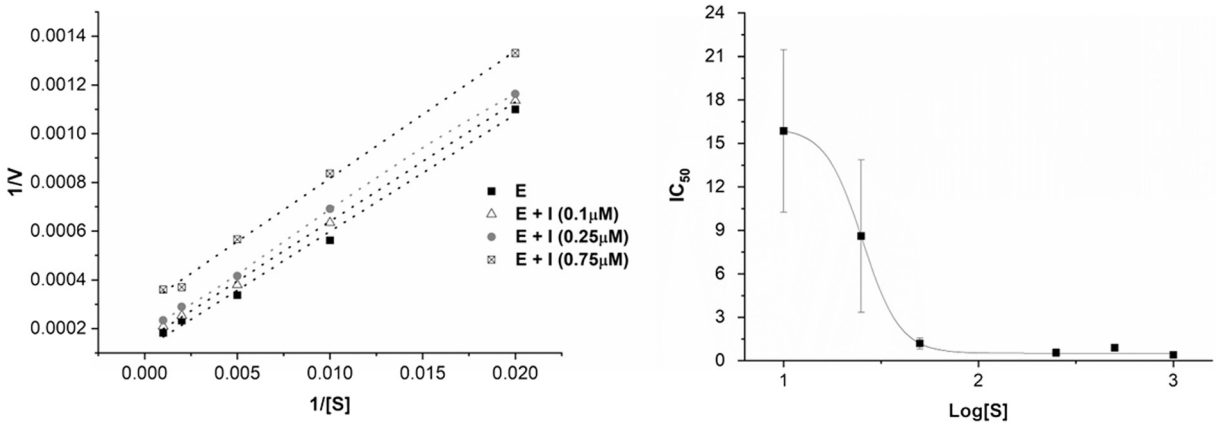

Fig. 4 Left: Lineweaver–Burk representation for the inhibition of SARS-CoV-2 PL^{pro} ("E") by the inhibitor **Ag-4b** ("I"); right: IC_{50} values for SARS-CoV-2 PL_{pro} inhibition by **Ag-4b** at different concentrations of substrate [S].

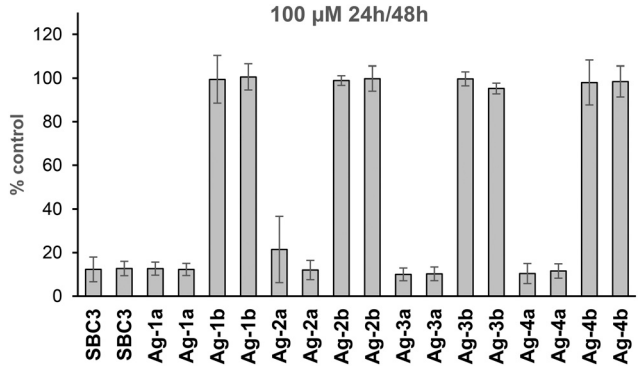

Fig. 5 Cytotoxicity of 100 µM of silver NHC complexes against almost confluent cell layers of Caco-2 cells (as % control of untreated cells). Left bars: 24 h, right bars: 48 h.

showed strong effects against the cells. Results with all other applied concentrations are given in the supporting info (see Fig. S6†). Notably, complex **Ag-4b** remained non-toxic up to 500 µM in these experiments.

Antiviral activity against SARS-CoV-2

Based on their favourable low or absent host cell cytotoxicity complexes **Ag-1b** to **Ag-4b** were selected for further evaluation of antiviral activity against authentic SARS-CoV-2 infection in Caco-2-F03 cells. The complexes were added simultaneously with the virus and the infection rate was determined by staining of spike protein after 24 h (see Fig. 6). All silver NHC complexes were effective antiviral agents that suppressed the infection at least by 50% starting at low micromolar non-toxic concentrations of roughly 0.5–20 µM. Only complexes **Ag-1b** and **Ag-3b** completely terminated viral activity at higher dosages, which however overlapped with toxicity in a parallel toxicity counter screen. Missing toxicity was again noted for **Ag-4b** and **Ag-2b** was moderately toxic only at very high dosage (CC_{50} values for both complexes >500 µM). **Ag-1b** to **Ag-3b** (IC_{50} values 6–18 µM) were effective antiviral agents and the by far most active compound was **Ag-4b** with an IC_{50} value of 0.58 µM.

Discussion and conclusions

Silver NHC complexes were prepared and evaluated as antiviral metallodrug candidates against SARS-CoV-2. Enzymatic inhibition studies confirmed a strong and selective inhibition of SARS-CoV-2 PL^{pro} with IC_{50} values below 0.5 µM. A rough comparison with IC_{50} values reported for different types of SARS-CoV-2 PL^{pro} inhibitors shows that the silver NHC complexes of this report are among the most effective

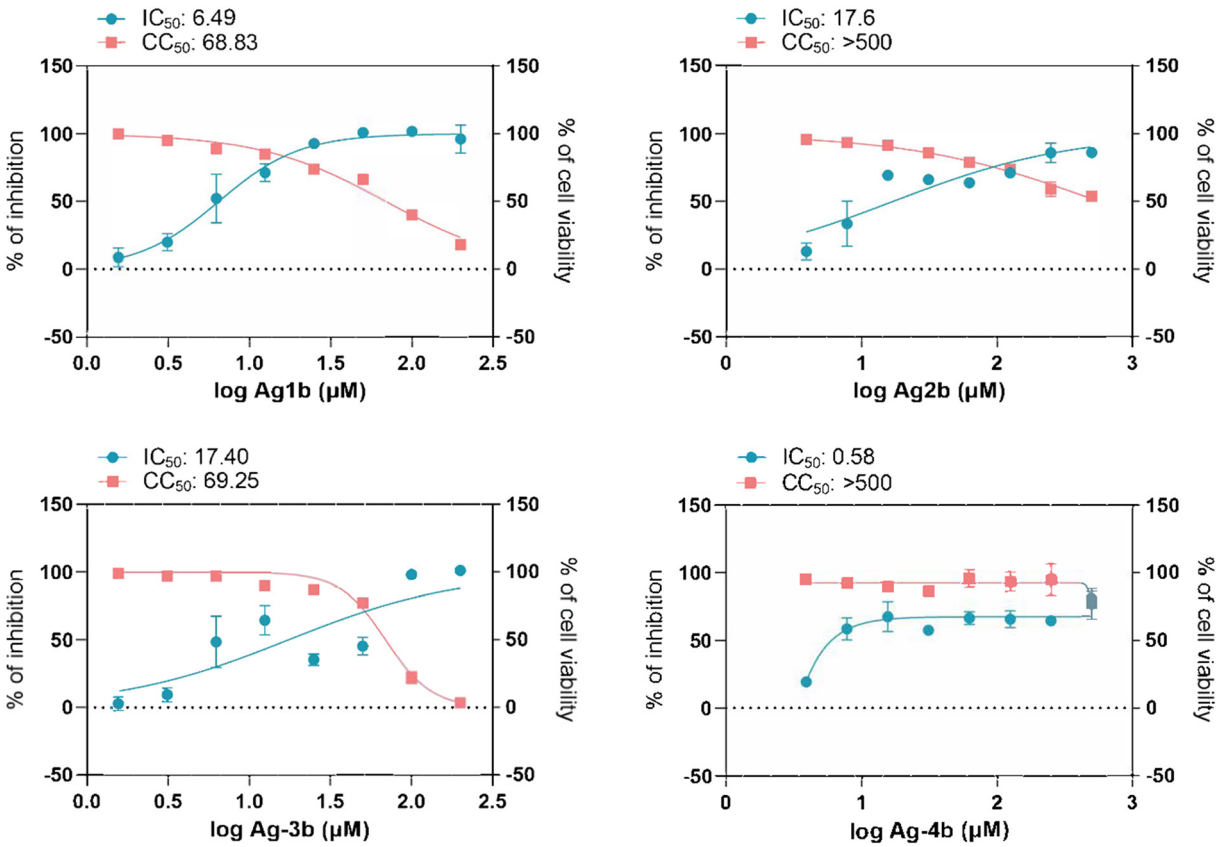

Fig. 6 Antiviral activity of silver compounds against SARS-CoV-2. Caco-F03 cells were treated with concentration range of silver compounds and subsequently infected with SARS-CoV-2 B.1 at MOI 0.01 or let uninfected. 24 h later the antiviral efficacy was determined by staining of spike protein and expressed as % of inhibition. The cell viability was determined by MTT assay. IC_{50} and CC_{50} values were calculated by Graphpad Prism 9.

inhibitors.[28] In contrast, their activity against SARS-CoV PL^{pro} was low and the complexes were inactive in experiments with SARS-CoV-2 $3CL^{pro}$, confirming that the complexes display a preference/selectivity for PL^{pro} from SARS-CoV-2 over other related proteases.

In our previous reports we could confirm activity against SARS-CoV-2 PL^{pro} also for gold and rhodium complexes as well as polyoxometalates.[8,11] Strong inhibition of this enzyme has also been reported for bismuth compounds[10] or zink pyrithione.[29] Inhibition of different SARS-CoV-2 enzymatic targets has been demonstrated for a small number of metal complexes, with helicase for bismuth[9,10] compounds, the spike/ACE2 interaction for titanocene dichloride and polyoxometalates,[8] $3CL^{pro}$ (M^{pro}) for bismuth,[10] rhenium,[30] zinc,[31] gold,[32] mercury[33] and ferrocene[34] complexes, and nsp14 N7-methyltansferase for gold and mercury complexes.[35]

PL^{pro} is a cysteine protease and in addition it hosts a zinc binding domain, in which the zinc is coordinated by four cysteine residues. Therefore, targeting the catalytic cysteine or the cysteines in the zinc binding domain is a promising strategy to inhibit the activity of this enzyme as it has been demonstrated with gold and other thiol-reactive probes, including disulfiram and ebselen.[11,25,26] Silver as a soft Lewis acid has a high affinity to soft bases such as thiolates. Zinc ejection experiments performed exemplarily with **Ag-4b** in fact confirmed efficacy comparable to that of disulfiram. Metal displacement has been suggested as a promising antiviral strategy and has been studied in detail for bismuth compounds with the enzyme helicase.[6,9,10] In general, zinc finger domains are considered as therapeutic targets for metal based compounds.[36] Also for silver compounds, although little explored in this aspect, zinc replacement from zinc finger binding sites has been reported.[37] Interestingly, Sun and colleagues recently confirmed zinc replacement from the colistin-resistance protein mcr-1 by silver ions in connection with the re-sensitisation of resistant bacteria to colistin.[38] It can therefore be speculated that zinc replacement could be a general mechanism of high relevance for silver-based anti-infectives.

Kinetic studies proved that **Ag-4b** exhibits an uncompetitive inhibition mechanism. This comparably rare mechanism of enzymatic inhibition explains that the inhibitor does not coordinate with the active centre of the enzyme, interacts with a different binding site, and binds only when the substrate has bound. Such mechanism is therefore also supportive of **Ag-4b** and other silver NHC complexes binding to the Zn binding domain of SARS-CoV-2 PL^{pro}. It is important to note that, as part of the uncompetitive binding mechanism, the affinity of **Ag-4b** for the preformed enzyme–substrate complex (K_i = 0.48 ± 0.22 μM) was approx. 4 orders of magnitude higher than the affinity for the enzyme before formation of the enzyme–substrate complex (K_m values: 411–176 μM). The development of inhibitors that show an uncompetitive mechanism brings significant pharmacological advantages. Due to fact that the inhibitor interacts only with the enzyme–substrate complex, it is only active when the enzyme is coordinated to the substrate, which provides high specificity and selectivity. The uncompetitive binding mechanism confirmed for **Ag-4b** might also explain the selectivity for PL^{pro} from SARS-CoV-2 over that from SARS-CoV (see Table 2). Similar selectivity had also been observed with other silver complexes in our previous report and it could therefore be speculated that uncompetitive PL^{pro} inhibition could be a general feature of silver complexes.[8]

A preliminary toxicity screening showed very low to absent toxicity for the iodido complexes **Ag-1b**–**Ag-4b**, while the chlorido analogues **Ag-1a**–**Ag-4a** were quite cytotoxic. This could be attributed to the higher stability (lower reactivity) of the iodido silver NHC complexes compared with the chlorido analogues.[19] Based on their favourable toxicity profile, **Ag-1b**–**Ag-4b** were selected for antiviral studies in SARS-CoV-2 infected cells. All complexes effectively suppressed SARS-CoV-2 viral replication at non-toxic low micromolar dosages with **Ag-4b** as the most active and completely non-toxic example.

Taken together, silver NHC complexes represent a promising novel type of SARS-CoV-2 PL^{pro} inhibitors with a rare uncompetitive binding mechanism and efficient antiviral efficacy at non-toxic concentration.

Experimental

General

Unless noted otherwise, all reagents were obtained from Sigma-Aldrich, VWR and Fluorochem and used as supplied. The purity of the synthesized compounds was proven by elemental analysis (Flash EA 1112, Thermo Quest) and differed by less than 0.5% from the predicted values. NMR spectra were recorded on a Bruker DRX-400 AS, AV III HD 500 or a AVII 600 NMR spectrometer; positive-ion ESI (electrospray ionization) mass spectra were recorded a expression^{L} CMS spectrometer (Advion). Complexes SBC3 (ref. 15) and **Ag-1a** (ref. 39) have been reported previously. Compounds 1,3-diethylbenzimidazolium iodide (**1**),[40] 1,3-di(isopropyl) benzimidazolium iodide (**3**),[41] 1,3-diethylbenzimidazolium chloride (**1a**)[42] and 1,3-di(isopropyl)benzimidazolium chloride (**3a**)[43] were reported in the literature already.

^{109}Ag-NMR spectroscopy

^{109}Ag-NMR spectra were recorded on a AV 300 MHz spectrometer and chemical shifts were referenced with respect to an external solution of 4.00 M silver nitrate in deuterium oxide (defined as δ 0 ppm). 100 mg (**Ag-4a**) or 120 mg (**Ag-4b**) were dissolved in 600 μL of d^6-DMSO. The AV 300 spectrometer was equipped with a PABBO BB-1H/DZ-GRD Z828401/0054, pulse sequence zg30, receiver gain 203.0, relaxation delay 20 s.

Synthesis

(Benz)imidazolium iodides 1–4. The requisite precursor (benz)imidazole was dissolved in acetonitrile (40 mL) and 1 equivalent of K_2CO_3 and 2.0 equivalents iodoethane or 3

equivalents 2-iodopropane were added. The reaction mixture was stirred under reflux conditions for 18 h (for **2** and **4**) or 3 days (for **1** and **3**). The solvent was evaporated and the residue was treated with dichloromethane. The suspension was filtered over Celite® to remove the K_2CO_3, the solvent was evaporated, and the residue was sonicated in ethyl acetate to produce a white or white off solid. The solid was filtered and dried under reduced pressure.

1,3-Diethyl-benzimidazolium iodide (1)[15]. The title compound was prepared according to the general procedure, starting from benzimidazole (1.181 g, 10 mmol). With a reaction period of 3 days. Yield: 37% (1.12 g, 3.7 mmol). ^{1}H NMR ($CDCl_3$, 600): 11.12 (s, 1H), 7.77 (m, 2H), 7.69 (m, 2H), 4.71 (q, 4H, J = 7.3 Hz), 1.78 (t, 6H, J = 7.3 Hz). ^{13}C NMR ($CDCl_3$, 151): 141.3, 131.1, 127.2, 113.0, 43.0, 14.8; elemental calculated for $C_{11}H_{15}N_2I$: C, 43.72; H, 5.00; N, 9.27; found: C, 43.87; H, 5.05; N, 9.58; MS (ESI+): m/z 175.3 $[M–I]^+$; MS (ESI −): m/z 127.1 $[I]^-$.

1,3-Diethyl-5-methoxy-benzimidazolium iodide (2). The title compound was prepared according to the general procedure starting from benzimidazole (0.445 g, 3 mmol) with a reaction period of 18 h; yield: 89% (0.887 g, 2.67 mmol); ^{1}H NMR ($CDCl_3$, 600 MHz): 10.93 (s, 1H, ArH2), 7.60 (d, 1H, J = 9.7 Hz, ArH7), 7.25 (dd, 1H, J = 9.7, 1.8 Hz, ArH6), 7.11 (d, 1H, J = 1.8 Hz, ArH4), 4.65 (m, 4H, 2× CH_2), 3.96 (s, 3H, OCH_3), 1.75 (m, 6H, 2× CH_3); ^{13}C NMR ($CDCl_3$, 151 MHz): 159.6 (ArC5), 140.4 (ArC2), 132.4 + 125.3 (ArC3 + ArC8), 117.4 (ArC), 113.7 (ArC), 95.2 (Ar), 56.4 (CH_3O), 43.0 (CH_2), 14.8 (CH_3); elemental analysis for $C_{12}H_{17}N_2OI$: calc.: C(43.39), H(5.16), N (8.43), found: C (43.37), H (5.18), N (8.39); MS (ESI +): m/z 205.1 $[M–I]^+$.

1,3-Diisopropyl-benzimidazolium iodide (3)[41]. The title compound was prepared according to the general procedure, starting from benzimidazole (0.591 g, 5 mmol). With a reaction period of 3 days. Yield: 72% (1.189 g, 3.39 mmol). ^{1}H NMR ($CDCl_3$, 600): 10.98 (s, 1H), 7.82 (m, 2H), 7.67 (m, 2H), 5.23 (hept, 2H, J = 6.8 Hz), 1.89 (d, 12H, J = 6.9 Hz).^{13}C NMR ($CDCl_3$, 151): 139.7, 130.8, 127.0, 113.9, 52.5, 22.2; MS (ESI+): m/z 203.3 $[M–I]^+$; MS (ESI−): m/z 127.1 $[I]^-$.

1,3-Diisopropyl-5-methoxy-benzimidazolium iodide (4). The title compound was prepared according to the general procedure starting from 5-methoxy-benzimidazole (1.482 g, 10 mmol) with a reaction period of 18 h. Yield: 74% (0.684 g, 1.9 mmol); ^{1}H NMR ($CDCl_3$, 600): 10.72 (s, 1H, ArH2), 7.68 (dd, 1H, J = 9.2, 0.6 Hz, ArH7), 7.24 (dd, 1H, J = 9.2, 2.3 Hz, ArH6), 7.18 (d, 1H, J = 2.3 Hz, ArH4) 5.17 (m, 2H, 2× CH), 3.97 (s, 3H, OCH_3), 1.86 (m, 12H, 4× CH_3); ^{13}C NMR ($CDCl_3$, 151): 159.3 (ArC5), 138.6 (ArC2), 132.1 + 124.8 (ArC3 + ArC8), 117.1 (ArC), 114.5 (ArC), 96.1 (ArC), 56.5 (CH), 52.4 (OCH_3), 52.0 (CH_3), 22.2 (CH_3); elemental for $C_{14}H_{21}N_2OI$: C, 46.68; H, 5.88; N, 7.78; found: C, 46.98; H, 5.82; N, 7.79; MS (ESI+): m/z 233.1 $[M–I]^+$.

(Benz)imidazolium chlorides (1a–4a). A flask was charged with the corresponding precursor (**1**–**4**) and dissolved in 20 mL of methanol with Amberlite® IRA402 chloride resin (1.000 g) and stirred at room temperature for 4 h. The reaction was then filtered under reduced pressure and the filtrate solvent removed under reduced pressure. The resulting oil was sonicated in 50 mL ethyl acetate to produce a white solid. The solid was filtered under reduced pressure and dried.

1,3-Diethyl-benzimidazolium chloride 1a (ref. 42). The title compound was prepared according to the general procedure, starting from 1,3-diethyl benzimidazolium iodide (0.250 g, 0.827 mmol). Yield: 97% (0.169 g, 0.802 mmol). ^{1}H NMR ($CDCl_3$, 500): 11.78 (s, 1H), 7.74 (dt, 2H, J = 6.4, 3.4 Hz), 7.67 (dt, 2H, J = 6.0, 3.4 Hz), 4.71 (q, 4H, J = 7.1 Hz), 1.74 (t, 6H, J = 7.3 Hz); ^{13}C NMR ($CDCl_3$, 126): 143.0, 131.2, 127.0, 112.9, 42.8, 14.9; MS (ESI+): m/z 175.2 $[M–Cl]^+$.

1,3-Diethyl-5-methoxy-benzimidazolium chloride 2a. The title compound was prepared according to the general procedure, starting from 1,3-diethyl-5-methoxy-benzimidazolium iodide (0.250 g 0.752 mmol). Yield: 92% (0.167 g 0.693 mmol). ^{1}H NMR (DMSO, 500) 11.50 (s, 1H, ArH2), 7.57 (d, 1H, J = 9.1 Hz, ArH7), 7.22 (dd, 1H, J = 9.1, 2.3 Hz, ArH6), 7.06 (d, 1H, J = 2.3 Hz, ArH4), 4.62 (m, 4H, 2× CH_2), 3.93 (s, 3H, OCH_3), 1.69 (m, 6H,2× CH_3); ^{13}C NMR ($CDCl_3$, 126): 159.2 (ArC5), 142.0 (ArC2), 132.1 + 125.2 (ArC3 + ArC8), 116.7 (ArC), 113.6 (ArC), 94.9 (ArC), 56.1 (OCH_3), 42.8 (CH_2), 42.6 (CH_2), 14.9 (CH_3), 14.8 (CH_3); MS (ESI+): m/z 205.3 $[M–Cl]^+$.

1,3-Diisopropyl-benzimidazolium chloride 3a (ref. 43). The title compound was prepared according to the general procedure, starting from 1,3-diisopropyl benzimidazolium iodide (0.250 g, 0.757 mmol). Yield:91% (0.186 g, 0.692 mmol). ^{1}H NMR ($CDCl_3$, 500): 11.86 (s, 1H), 7.78 (2H, m), 7.64 (dt, 2H, J = 6.3, 3.3 Hz), 5.20 (hept, 2H, J = 6.9 Hz), 1.87 (d, 12H, J = 6.9 Hz). ^{13}C NMR ($CDCl_3$, 126): 141.6, 130.8, 126.7, 113.7, 52.2, 22.1; MS (ESI+): m/z 203.3 $[M–Cl]^+$.

1,3-Diisopropyl-5-methoxy-benzimidazolium chloride 4a. The title compound was prepared according to the general procedure, starting from 1,3-diisopropyl-5-methoxy-benzimidazolium iodide (0.250 g, 0.694 mmol). Yield: 81% (0.151 g, 0.562 mmol); ^{1}H NMR ($CDCl_3$, 400 MHz): 11.68 (s, 1H, ArH2), 7.65 (d, 1H, J = 9.7 Hz, ArH7), 7.22 (dd, 1H, J = 9.7, 2.3 Hz, ArH6), 7.12 (d, 1H, J = 2.3 Hz, ArH4), 5.12 (m, 2H, 2× CH), 3.95 (s, 3H, OCH_3), 1.84 (m, 12H, 2× CH_3).^{13}C NMR ($CDCl_3$, 101 MHz): 159.0 (ArC5), 140.8 (ArC2), 132.0 + 124.0 (ArC3 + ArC8), 116.5 (ArC), 114.4 (ArC), 96.0 (ArC), 56.2 (OCH_3), 52.3 (CH), 51.8 (CH), 22.2 (CH_3), 22.1 (CH_3); elemental calculated for $C_{14}H_{21}N_2OCl$: C, 62.56; H, 7.88; N, 10.42; found: C, 62.01; H, 7.91; N, 10.21; MS (ESI+): m/z 233.1 $[M–Cl]^+$.

General procedure for synthesis of NHC–Ag–X complexes

A flask was charged with the corresponding (benz) imidazolium precursor and silver oxide (0.6 equivalents) and stirred in dried dichloromethane for 2 h (for **Ag-1b**, **Ag-2a**, **Ag-2b**, **Ag-3b**) or 18 h (for **Ag-1a**, **Ag-3a**, **Ag-4a**, **Ag-4b**) at 40 °C in the dark. The reaction mixture was filtered through a bed of celite, the filtrate was reduced to 5 mL and 50 mL of pentane were added to precipitate a solid. The solid was isolated by filtration under reduced pressure and dried.

1,3-Diethyl benzimidazolium silver(I) chloride (Ag-1a)[39]. The title compound was prepared according to the general procedure starting from 1,3-diethyl benzimidazolium chloride (0.100 g, 0.476 mmol). Yield: 56% (84.5 mg, 0.268 mmol), white powder; ^{1}H NMR (DMSO, 500 MHz): 7.83 (m, 2H, ArH), 7.46 (m, 2H, ArH), 4.50 (q, 4H, J = 7.3 Hz, 2× CH_2), 1.44 (t, 6H, J = 7.3 Hz, 2× CH_3). ^{13}C NMR (DMSO, 126 MHz): 186.5 (ArC2), 132.5 (ArC3), 123.7 (ArC), 111.5 (ArC), 43.7 (CH_2), 15.7 (CH_3); elemental: calculated for $C_{11}H_{14}N_2AgCl$: C, 41.60; H, 4.44; N, 8.82; found: C, 41.69; H, 4.36; N, 8.67. MS (ESI+): m/z 175.2 $[M–Ag–Cl]^+$, 455.5 $[M–Cl + NHC]^+$; MS(ESI−): m/z 177.0 $[AgCl_2]^-$.

1,3-Diethyl-5-methoxy-benzimidazolium silver(I) chloride (Ag-2a). The title compound was prepared according to the general procedure, starting from 1,3-diethyl-5-methoxy-benzimidazolium chloride (0.100 g 0.415 mmol). Yield: 40% (0.057 g 0.166 mmol) white off powder; ^{1}H NMR (DMSO, 500) 7.7 (d, 1H, J = 9.1 Hz, ArH7), 7.3 (d, 1H, J = 2.3 Hz, ArH4), 7.06 (dd, 1H, J = 9.1, 2.3 Hz, ArH6), 4.62 (m, 4H, 2× CH_2), 3.93 (s, 3H, OCH_3), 1.69 (m, 6H, 2× CH_3); ^{13}C NMR (DMSO, 126): C2 not detected, 156.8 (ArC5), 133.7 + 127.0 (ArC3 + ArC8), 112.9 (ArC), 112.6 (ArC), 95.3 (ArC), 55.8 (OCH_3), 43.8 (CH_2), 43.4 (CH_2), 15.9 (CH_3), 15.8 (CH_3); elemental calculated for $C_{12}H_{16}N_2OAgCl$: C, 41.46; H, 4.64; N, 8.06; found: C, 41.51; H, 4.72; N, 8.00; MS (ESI+): m/z 205.3 $[M–Ag–Cl]^+$, 515.4 $[M–Cl + NHC]^+$; MS (ESI−): m/z 177.0 $[AgCl_2]^-$.

1,3-Diisopropyl benzimidazolium silver(I) chloride (Ag-3a). The title compound was prepared according to the general procedure starting from 1,3-diisopropyl-benzimidazolium chloride (0.100 g, 0.419 mmol) yield: 63% (91 mg, 0.181 mmol), white powder; ^{1}H NMR (DMSO, 500): 7.93 (m, 2H, ArH), 7.42 (m, 2H, ArH), 5.10 (hept, 2H, J = 6.9 Hz, 2× CH), 1.67 (d, 12H, J = 6.9 Hz, 2× CH_3);^{13}C NMR (DMSO, 126): 183.2 (ArC2), 132.4 (ArC3), 123.6 (ArC), 112.7 (ArC), 52.3 (CH), 22.2 (CH_3); elemental calculated for $C_{13}H_{18}N_2AgCl$: C, 45.18; H, 5.25; N, 8.11; found: C, 45.29; H, 5.26; N, 8.06. MS (ESI+): m/z 203.1 $[M–Ag–Cl]^+$, 511.1 $[M–Cl + NHC]^+$; MS (ESI−): m/z 176.8 $[AgCl_2]^-$.

1,3-Diisopropyl-5-methoxy-benzimidazolium silver(I) chloride (Ag-4a). The title compound was prepared according to the general procedure starting from 1,3-diisopropyl-5-methoxy-benzimidazolium chloride (0.100 g, 0.372 mmol). Yield: 69% (96 mg, 0.208 mmol), white powder; ^{1}H NMR (DMSO, 500): 7.80 (d, 1H, J = 9.0 Hz, ArH7), 7.39 (d, 1H, J = 2.3 Hz, ArH4), 7.02 (dd, 1H, J = 9.0, 2.3 Hz, ArH6), 5.04 (m, 2H, 2× CH), 3.31 (s, 3H, OCH_3), 1.66 (m, 12H, CH_3); ^{13}C NMR (DMSO, 126): 182.0 (ArC2), 156.4 (ArC5), 133.7 + 126.5 (ArC3 + ArC8), 113.3 (ArC), 112.5 (ArC), 95.6 (ArC), 55.6 (OCH_3), 52.6 (CH), 51.0 (CH), 22.5 (CH_3), 22.3 (CH_3); elemental for $C_{14}H_{20}N_2AgClO$: C, 44.76; H, 5.37; N, 7.46; found: C, 45.06; H, 5.34; N, 7.15; MS (ESI+): m/z 233.1 $[M–Ag–Cl]^+$, 571.1 $[M–Cl + NHC]^+$; MS (ESI−): m/z 176.8 $[AgCl_2]^-$.

1,3-Diethyl-benzimidazolium silver(I) iodide (Ag-1b). The title compound was prepared according to the general procedure, starting from 1,3-diethyl-benzimidazolium iodide (0.100 g, 0.331 mmol). Yield: 48% (64 mg, 0. 157 mmol), white powder; ^{1}H NMR (DMSO, 500): 7.84 (s, 2H, ArH), 7.47 (m, 2H, ArH), 4.57 (q, 4H, J = 7.2 Hz, 2× CH_2), 1.48 (t, 6H, J = 7.2 Hz, 2× CH_3); ^{13}C NMR (DMSO, 126): 189.5 (ArC2), 132.8 (ArC3), 123.7 (ArC), 111.8 (ArC), 43.5 (CH_2), 15.9 (CH_3); elemental calculated for $C_{11}H_{14}N_2AgI$: C, 32.30; H, 3.45; N, 6.85; found: C, 32.86; H, 3.53; N, 6.79; MS (ESI+): m/z 175.0 $[M–Ag–I]^+$, 455.0 $[M–I + NHC]^+$; MS (ESI−): m/z 126.9 $[I]^-$, 360.7 $[AgI_2]^-$.

1,3-Diethyl-5-methoxy-benzimidazolium silver(I) iodide (Ag-2b). The title compound was prepared according to the general procedure, starting from 1,3-diethyl-5-methoxy-benzimidazolium iodide (0.100 g, 0.301 mmol). Yield: 71% (94 mg, 0.215 mmol), white powder; ^{1}H NMR (DMSO, 500): 7.71 (d, 1H, J = 8.9 Hz, ArH7), 7.37 (d, 1H, J = 2.3 Hz, ArH4), 7.05 (dd, 1H, J = 8.9, 2.3 Hz, ArH6), 4.51 (m, 4H, 2× CH_2), 3.87 (s, 3H, OCH_3), 1.46 (m, 6H, 2× CH_3); ^{13}C NMR (DMSO, 126): 188.8 (ArC2), 156.9 (ArC5), 133.9 +127.5 (ArC3 + ArC8), 112.8 (ArC), 112.45 (ArC), 95.2 (ArC), 55.8 (OCH_3), 43.5 (CH_2), 43.2 (CH_2), 16.0 (CH_3), 15.9 (CH_3); elemental calculated for $C_{12}H_{16}N_2AgOI$: C, 32.83; H, 3.67; N, 6.38; found: C, 33.26; H, 3.69; N, 6.42; MS (ESI+): m/z 205.1 $[M–Ag–I]^+$, 515.1 $[M–I + NHC]^+$; MS (ESI−): m/z 126.9 $[I]^-$, 360.7 $[AgI_2]^-$.

1,3-Diisopropyl benzimidazolium silver(I) iodide (Ag-3b). The title compound was prepared according to the general procedure starting from 1,3-diisopropyl-benzimidazolium iodide (0.100 g, 0.303 mmol). Yield: 60% (79 mg, 0.181 mmol), light brown powder; ^{1}H NMR (DMSO, 500): 7.95 (m, 2H, ArH), 7.44 (m, 2H, ArH), 5.18 (hept, 2H, J = 7.0 Hz, 2× CH), 1.71 (d, 12H, J = 7.0 Hz, 4× CH_3); ^{13}C NMR (DMSO, 126): 185.8 (ArC2), 132.4 (ArC3), 123.6 (ArC), 112.7 (ArC), 52.2 (CH), 22.3 (CH_3); elemental calculated for $C_{13}H_{18}N_2AgI$: C, 35.72; H, 4.15; N, 6.41; found: C, 35.68; H, 4.22; N, 6.04; MS (ESI+): m/z 203.0 $[M–Ag–I]^+$, $[M–I + NHC]^+$ = 511.1; MS (ESI−): m/z 126.9 $[I]^-$, 360.6 $[AgI_2]^-$.

1,3-Diisopropyl-5-methoxy-benzimidazolium silver(I) iodide (Ag-4b). The title compound was prepared according to the general procedure, starting from 1,3-diisopropyl-5-methoxy-benzimidazolium iodide (0.100 g, 0.278 mmol). Yield: 74% (97 mg, 0.208 mmol), white powder; ^{1}H NMR (DMSO, 500): 7.81 (d, 1H, J = 8.7 Hz, ArH7), 7.40 (d, 1H, J = 2.4 Hz, ArH4), 7.03 (dd, 1H, J = 8.7, 2.4 Hz, ArH6), 5.11 (m, 2H, 2× CH), 3.87 (s, 3H, OCH_3), 1.68 (m, 12H, 4× CH_3);^{13}C NMR (DMSO, 126): 184.8 (ArC2), 156.5 (ArC5), 133.8 + 126.5 (ArC3 + ArC8), 113.18 (ArC), 112.62 (ArC), 95.92 (ArC), 55.81 (OCH_3), 52.46 (CH), 51.07 (CH), 22.53 (CH_3), 22.37 (CH_3); elemental calculated for $C_{14}H_{20}N_2AgOI$: C, 36.00; H, 4.32; N, 6.00; found: C, 36.07; H, 4.23 N, 5.66; MS (ESI+): m/z 233.1 $[M–Ag–I]^+$, 571.1 $[M–I + NHC]^+$; MS (ESI−): m/z 126.9 $[I]^-$, 360.6 $[AgI_2]^-$.

Conductometry

Conductivity measurements were performed using an Apera Instruments EC9500 conductivity meter. Solutions (1.0 mM, or as indicated) of all compounds were prepared using freshly distilled DMSO with a relative electric conductivity of

$\leq 3 \times 10^{-8}$ Ω cm^{-1}. The conductivities were measured at 25 ± 2 °C immediately after complete dissolution, after 24 h, and after 48 h.

SARS-CoV-2 and SARS-CoV PL^{pro} inhibition

The inhibition of PLpro was determined as previously described.[11] The inhibitor compounds were prepared as stock solutions in DMSO and diluted hundredfold with HEPES buffer (50 mm HEPES, pH 7.5, 0.1 mg mL^{-1} bovine serum albumin, 0.1% Triton-X100) to micromolar concentrations. Volumes of 50 μL of 200 nM SARS-CoV-2 PL^{pro} (Elabscience)/ His6-SARS-CoV-1 PL^{pro} (South Bay Bio) in HEPES buffer or blank HEPES buffer (negative control) were added to the wells of a black 96-well microtiter plate (Greiner Bio One). Volumes of 50 μL of the inhibitor solutions or 1% DMSO in HEPES buffer (positive control) were added. The resulting solutions (100 nm SARS-CoV-2 PL^{pro}/His6-SARS-CoV-1 PL^{pro}, 0.5% DMSO, 0.1–100 μm test compound or blank HEPES buffer) were mixed and incubated at 37 °C for one hour. A volume of 100 μL of 100 mm Z-Arg-Leu-Arg-Gly-Gly-AMC (Bachem) was added to all wells. The resulting solutions were mixed and the fluorescence emission was measured immediately every 30 s for 10 min (λ_{exc} = 355 nm; λ_{em} = 460 nm) at 37 μC using a VictorTM X4 Perkin Elmer 2030 multilabel reader. The increase of emission over time followed a linear trend (r^2 >0.97) and the enzymatic activities were calculated as the slope thereof. The IC_{50} values were calculated as the concentration of the inhibitor that was required to decrease the enzymatic activity to 50% of the positive control. The wells containing the negative control were used to confirm the absence of false positive results by reaction of the inhibitor compound with the fluorogenic substrate.

Zn-Ejection assay SARS-CoV-2 PL^{pro} inhibition

To determine if the inhibitors are Zn-ejecting agents, the presence of free Zn^{2+} in solution was measured as previously described.[11] The inhibitor compounds were prepared as stock solutions in DMSO and diluted hundredfold with HEPES buffer (50 mM HEPES, pH 7.5) to 2 μM and 20 μM concentrations. Volumes of 50 μL of 1 μM SARS-CoV-2 PL^{pro} (Elabscience) in HEPES buffer or blank HEPES buffer (negative control) were added to the wells of a black 96-well microtiter plate (Greiner Bio One). Volumes of 50 μL of the inhibitor solutions or 1% DMSO in HEPES buffer (positive control) were added. The resulting solutions (500 nM PL^{pro} SARS-CoV-2, 0.5% DMSO, 1 μM or 10 μM test compound or blank HEPES buffer) were mixed. A volume of 100 μL of 2.0 μM of zinc-specific fluorophore FluoZinTM-3 (Invitrogen/Life Technologies) was added to all wells. The resulting solutions were mixed and the fluorescence emission was measured immediately every 5 min for 100 min (λ_{exc} = 485 nm; λ_{em} = 535 nm) at 37 °C using a Victor™ X4 Pekin Elmer 2030 multilabel reader. The wells containing the negative control were used to confirm the absence of false positive results by reaction of the inhibitor compound with the zinc-specific fluorophore.

Michaelis–Menten kinetics with SARS-CoV-2 PL^{pro}

The inhibitor compounds were prepared as stock solutions in DMSO and diluted hundredfold with HEPES buffer (50 mm HEPES, pH 7.5, 0.1 mg mL^{-1} bovine serum albumin, 0.1% Triton-X100) to micromolar concentrations. Volumes of 50 μL of 200 nM SARS-CoV-2 PL^{pro} (Elabscience) in HEPES buffer were added to the wells of a black 96-well microtiter plate (Greiner Bio One). Volumes of 50 μL of the inhibitor solutions or 1% DMSO in HEPES buffer (positive control) were added. The resulting solutions (100 nm SARS-CoV-2 PL^{pro} 0.5% DMSO, 0.1–0.75 μm test compound or blank HEPES buffer) were mixed and incubated at 37 °C for 10 min. A volume of 100 μL of 20–8000 μm of substrate (Z-Arg-Leu-Arg-Gly-Gly-AMC, Bachem) was added to all wells. The resulting solutions were mixed and the fluorescence emission was measured immediately every minute for 1 h (λ_{exc} = 355 nm; λ_{em} = 460 nm) at 37 °C using a Victor™ X4 Perkin Elmer 2030 multilabel reader. The enzyme activity of PL^{pro} was represented by the Michaelis Menten equation (eqn (1)) and the K_m and V_{max} values were calculated with Lineweaver–Burk equation (eqn (2)) where the slope is K_m/V_{max}, the intersection with the *Y*-axis corresponds to $1/V_{max}$, and intersection with the *X*-axis corresponds to $-1/K_m$.

$$V = \frac{V_{max}[S]}{k_m + [S]} \quad (1)$$

$$\frac{1}{V} = \frac{k_m}{V_{max}}\frac{1}{[S]} + \frac{1}{V_{max}} \quad (2)$$

SARS-CoV-2 $3CL^{pro}$ inhibition

The inhibition of $3CL^{pro}$ was determined according to reported protocols with modifications.[44] The inhibitor compounds were prepared as stock solutions in DMSO and diluted hundredfold with HEPES buffer (50 mM HEPES, pH 7.5, 0.1 mg mL^{-1} bovine serum albumin, 0.1% Triton-X100, 0.1 mM DTT) to micromolar concentrations. Volumes of 50 μL of 200 nM MBP-tag SARS-CoV-2 $3CL^{pro}$ (Bioscience) in HEPES buffer or blank HEPES buffer (negative control) were added to the wells of a black 96-well microtiter plate (Greiner Bio One). Volumes of 50 μL of the inhibitor solutions or 1% DMSO in HEPES buffer (positive control) were added. The resulting solutions (100 nM SARS-CoV-2 $3CL^{pro}$, 0.5% DMSO, 100 μm test compound or blank HEPES buffer) were mixed and incubated at 37 °C for one hour. A volume of 100 μL of 100 μM DABCYL-KTSAVLQSGFRKME-EDANS (Bachem) was added to all wells. The resulting solutions were mixed and the fluorescence emission was measured immediately every 3 min for 75 min (λ_{exc} = 355 nm; λ_{em} = 460 nm) at 37 °C using a Victor™ X4 Perkin Elmer 2030 multilabel reader. The increase of emission over time followed a linear trend (r^2

>0.97) and the enzymatic activities were calculated as the slope thereof. The wells containing the negative control were used to confirm the absence of false positive results by reaction of the inhibitor compound with the fluorogenic substrate.

Toxicity against host cells (CaCo-2)

Caco-2 cells were grown as almost confluent monolayers in 96 well plates. The complexes were dissolved as stock solutions in DMSO (0.2%) diluted with DMEM cell culture medium, which was supplemented with 1% fetal calf serum and 50 mg L^{-1} gentamicin. The cell layers were incubated with the drug containing media for 24 h and 48 h at 37 °C/5% CO_2 in an incubator. The cell viability was determined by crystal violet staining and cell viability was calculated as percentage of an untreated control. Results were obtained in three independent experiments.

Antiviral effects against SARS-CoV-2

Cell lines. Caco-2-F03, subline of human colon carcinoma cell line Caco-2, which was previously clonally selected to obtain cell line[45] highly permissive for coronavirus infection was grown at 37 °C in minimal essential medium (MEM) supplemented with 10% fetal bovine serum (FBS) and containing 100 IU mL^{-1} penicillin and 100 μg mL^{-1} streptomycin. All culture reagents were purchased from Sigma. The cells have been tested negative for mycoplasma infection.

Virus isolation and preparation

SARS-CoV-2 B.1 (SARS-CoV-2/FFM7, MT358643) was isolated from naso-pharyngeal swabs of COVID-19 patients using subline Caco-2-F03. SARS-CoV-2 stocks used in the experiments had undergone two passages and were stored at −80 °C. Virus titers were determined as TCID50 per mL in confluent cells in 96-well microtiter plates. The isolate was authenticated and the sequence is publicly available at **https://GISAID.org**.

Antiviral activity of silver compounds

Confluent layers of Caco-2-F03 were infected with SARS-CoV-2 B.1 at a MOI of 0.01. The tested compounds were added simultaneously with virus and incubated in MEM supplemented with 1% FBS. Immunohistochemistry of viral spike protein was performed after 24 h post infection to determine antiviral activity against SARS-CoV-2 infection.

Immunohistochemistry

Cells were fixed with acetone : methanol (40 : 60) solution and immunostaining was performed using a monoclonal antibody directed against the S protein of SARS-CoV-2 (1 : 1500, Sinobiological), which was detected with a peroxidase-conjugated anti-rabbit secondary antibody (1 : 1000, Dianova), followed by addition of AEC substrate. The S positive area was scanned and quantified by automated plate reader. The results were expressed as percentage of infection relative to virus control which received no drug.

Cell viability assay

Cell viability was measured by 3-(4,5-dimethylthiazol-2-yl)-2,5-diphenyltetrazolium bromide (MTT) dye reduction assay. 25 μL of MTT solution (2 mg mL^{-1} in PBS) were added per well, and the plates were incubated at 37 °C for 4 h. After this, the cells were lysed using 100 μL of a buffer containing 20% sodium dodecylsulfate and 50% *N*,*N*-dimethylformamide with the pH adjusted to 4.7 at 37 °C for 4 h. Absorbance was determined at 560 nm (reference wavelength 620 nm) using a Tecan infinite M200 microplate reader (TECAN).

Conflicts of interest

There is no conflict of interest to declare.

Acknowledgements

M. G.-M. acknowledges support by a Margarita-Salas-Fellowship (European Union, NextGenerationEU), I. V. E. acknowledges support by a Georg-Christoph-Lichtenberg-Fellowship by the Ministry of Science and Culture of the State of Lower-Saxony within the graduate program iCA ("Drug Discovery and Cheminformatics for New Anti-Infectives"). We thank Kerstin Euler, Sebastian Grothe and Lena Stegmann for their technical support.

References

1 (*a*) I. Ott and R. Gust, *Arch. Pharm.*, 2007, **340**, 117; (*b*) G. Gasser, I. Ott and N. Metzler-Nolte, *J. Med. Chem.*, 2011, **54**, 3–25.
2 K. D. Mjos and C. Orvig, *Chem. Rev.*, 2014, **114**, 4540–4563.
3 A. Frei, J. Zuegg, A. G. Elliott, M. Baker, S. Braese, C. Brown, F. Chen, C. G. Dowson, G. Dujardin, N. Jung, A. P. King, A. M. Mansour, M. Massi, J. Moat, H. A. Mohamed, A. K. Renfrew, P. J. Rutledge, P. J. Sadler, M. H. Todd, C. E. Willans, J. J. Wilson, M. A. Cooper and M. A. T. Blaskovich, *Chem. Sci.*, 2020, **11**, 2627–2639.
4 R. E. F. de Paiva, A. Marçal Neto, I. A. Santos, A. C. G. Jardim, P. P. Corbi and F. R. G. Bergamini, *Dalton Trans.*, 2020, **49**, 16004–16033.
5 (*a*) T. Marzo and L. Messori, *ACS Med. Chem. Lett.*, 2020, **11**, 1067–1068; (*b*) J. Karges and S. M. Cohen, *ChemBioChem*, 2021, 2600–2607; (*c*) K. Ioannou and M. C. Vlasiou, *BioMetals*, 2022, **35**(4), 639–652.
6 H. Li, S. Yuan, X. Wei and H. Sun, *Chem. Commun.*, 2022, **58**, 7466.
7 (*a*) H. A. Rothan, S. Stone, J. Natekar, P. Kumari, K. Arora and M. Kumar, *Virology*, 2020, **547**, 7; (*b*) D. Cirri, T. Marzo, I. Tolbatov, A. Marrone, F. Saladini, I. Vicenti, F. Dragoni, A. Boccuto and L. Messori, *Biomolecules*, 2021, **11**, 1858; (*c*) C. Chuong, C. M. DuChane, E. M. Webb, P. Rai, J. M. Marano, C. M. Bernier, J. S. Merola and J. Weger-Lucarelli, *Viruses*, 2021, **13**, 980.

8 M. Gil-Moles, S. Türck, U. Basu, A. Pettenuzzo, S. Bhattacharya, A. Rajan, X. Ma, R. Büssing, J. Wölker, H. Burmeister, H. Hoffmeister, P. Schneeberg, A. Prause, P. Lippmann, J. Kusi-Nimarko, S. Hassell-Hart, A. McGown, D. Guest, Y. Lin, A. Notaro, R. Vinck, J. Karges, K. Cariou, K. Peng, X. Qin, X. Wang, J. Skiba, Ł. Szczupak, K. Kowalski, U. Schatzschneider, C. Hemmert, H. Gornitzka, E. R. Milaeva, A. A. Nazarov, G. Gasser, J. Spencer, L. Ronconi, U. Kortz, J. Cinatl, D. Bojkova and I. Ott, *Chem. – Eur. J.*, 2021, **27**, 17928–17940.

9 S. Yuan, R. Wang, J. F.-W. Chan, A. J. Zhang, T. Cheng, K. K.-H. Chik, Z.-W. Ye, S. Wang, A. C.-Y. Lee, L. Jin, H. Li, D.-Y. Jin, K.-Y. Yuen and H. Sun, *Nat. Microbiol.*, 2020, **5**, 1439–1448.

10 R. Wang, J. F.-W. Chan, S. Wang, H. Li, J. Zhao, T. K.-Y. Ip, Z. Zuo, K.-Y. Yuen, S. Yuan and H. Sun, *Chem. Sci.*, 2022, **13**, 2238–2248.

11 M. Gil-Moles, U. Basu, R. Büssing, H. Hoffmeister, S. Türck, A. Varchmin and I. Ott, *Chem. – Eur. J.*, 2020, **26**, 15140–15144.

12 (*a*) C. Ma, M. D. Sacco, Z. Xia, G. Lambrinidis, J. A. Townsend, Y. Hu, X. Meng, T. Szeto, M. Ba, X. Zhang, M. Gongora, F. Zhang, M. T. Marty, Y. Xiang, A. Kolocouris, Y. Chen and J. Wang, *ACS Cent. Sci.*, 2021, **7**, 1245–1260; (*b*) Z. Shen, K. Ratia, L. Cooper, D. Kong, H. Lee, Y. Kwon, Y. Li, S. Alqarni, F. Huang, O. Dubrovskyi, L. Rong, G. R. J. Thatcher and R. Xiong, *J. Med. Chem.*, 2022, **65**, 2940–2955.

13 (*a*) A. Melaiye, R. S. Simons, A. Milsted, F. Pingitore, C. Wesdemiotis, C. A. Tessier and W. J. Youngs, *J. Med. Chem.*, 2004, **47**, 973–977; (*b*) K. M. Hindi, M. J. Panzner, C. A. Tessier, C. L. Cannon and W. J. Youngs, *Chem. Rev.*, 2009, **109**, 3859.

14 (*a*) C. L. Cannon, L. A. Hogue, R. K. Vajravelu, G. H. Capps, A. Ibricevic, K. M. Hindi, A. Kascatan-Nebioglu, M. J. Walter, S. L. Brody and W. J. Youngs, *Antimicrob. Agents Chemother.*, 2009, **53**, 3285–3293; (*b*) K. M. Hindi, A. J. Ditto, M. J. Panzner, D. A. Medvetz, D. S. Han, C. E. Hovis, J. K. Hilliard, J. B. Taylor, Y. H. Yun, C. L. Cannon and W. J. Youngs, *Biomaterials*, 2009, **30**, 3771; (*c*) N. A. Johnson, M. R. Southerland and W. J. Youngs, *Molecules*, 2017, **22**, 1263; (*d*) J. O'Loughlin, S. Napolitano, F. Alkhathami, C. O'Beirne, D. Marhöfer, M. O'Shaughnessy, O. Howe, M. Tacke and M. Rubini, *ChemBioChem*, 2021, **22**, 1093–1098; (*e*) W. Streciwilk, J. Cassidy, F. Hackenberg, H. Müller-Bunz, F. Paradisi and M. Tacke, *J. Organomet. Chem.*, 2014, **749**, 88; (*f*) S. A. Patil, S. A. Patil, R. Patil, R. S. Keri, S. Budagumpi, G. R. Balakrishna and M. Tacke, *Future Med. Chem.*, 2015, **7**, 1305–1333; (*g*) C. O'Beirne, H. T. Althani, O. Dada, J. Cassidy, K. Kavanagh, H. Müller-Bunz, Y. Ortin, X. Zhu and M. Tacke, *Polyhedron*, 2018, **149**, 95–103.

15 S. Patil, A. Deally, B. Gleeson, H. Müller-Bunz, F. Paradisi and M. Tacke, *Metallomics*, 2011, **3**, 74–88.

16 O. Sánchez, S. González, Á. R. Higuera-Padilla, Y. León, D. Coll, M. Fernández, P. Taylor, I. Urdanibia, H. R. Rangel, J. T. Ortega, W. Castro and M. C. Goite, *Polyhedron*, 2016, **110**, 14–23.

17 H. M. J. Wang and I. J. B. Lin, *Organometallics*, 1998, **17**, 972–975.

18 (*a*) M. V. Baker, P. J. Barnard, S. K. Brayshaw, J. L. Hickey, B. W. Skelton and A. H. White, *Dalton Trans.*, 2005, 37–43; (*b*) H. V. Huynh, Y. Han, R. Jothibasu and J. A. Yang, *Organometallics*, 2009, **28**, 5395–5404.

19 J. C. Garrison and W. J. Youngs, *Chem. Rev.*, 2005, **105**, 3978–4008.

20 (*a*) L. Busetto, M. C. Cassani, C. Femoni, A. Macchioni, R. Mazzoni and D. Zuccaccia, *J. Organomet. Chem.*, 2008, **693**, 2579–2591; (*b*) P. de Frémont, N. M. Scott, E. D. Stevens, T. Ramnial, O. C. Lightbody, C. L. B. Macdonald, J. A. C. Clyburne, C. D. Abernethy and S. P. Nolan, *Organometallics*, 2005, **24**, 6301–6309.

21 U. Hintermair, U. Englert and W. Leitner, *Organometallics*, 2011, **30**, 3726–3731.

22 T. Ramnial, C. D. Abernethy, M. D. Spicer, I. D. McKenzie, I. D. Gay and J. A. C. Clyburne, *Inorg. Chem.*, 2003, **42**, 1391–1393.

23 A. J. Arduengo, H. V. R. Dias, J. C. Calabrese and F. Davidson, *Organometallics*, 1993, **12**, 3405–3409.

24 B. Bildstein, M. Malaun, H. Kopacka, K. Wurst, M. Mitterböck, K.-H. Ongania, G. Opromolla and P. Zanello, *Organometallics*, 1999, **18**, 4325–4336.

25 B. K. Maiti, *ACS Pharmacol. Transl. Sci.*, 2020, **3**, 1017–1019.

26 K. Sargsyan, C.-C. Lin, T. Chen, C. Grauffel, Y.-P. Chen, W.-Z. Yang, H. S. Yuan and C. Lim, *Chem. Sci.*, 2020, **11**, 9904–9909.

27 T. P. Kenakin, Enzymes as Drug Targets, *Pharmacology in Drug Discovery*, ed. T. P. Kenakin, Academic Press, 2012, ch. 6, pp. 105–124.

28 H. Tan, Y. Hu, P. Jadhav, B. Tan and J. Wang, *J. Med. Chem.*, 2022, **65**, 7561–7580.

29 J. Kladnik, A. Dolinar, J. Kljun, D. Perea, J. Grau-Expósito, M. Genescà, M. Novinec, M. J. Buzon and I. Turel, *J. Enzyme Inhib. Med. Chem.*, 2022, **37**, 2158–2168.

30 (*a*) J. Karges, M. Kalaj, M. Bembicky and S. M. Cohen, *Angew. Chem., Int. Ed.*, 2021, **60**, 10716–10723; (*b*) J. Karges and S. M. Cohen, *J. Med. Chem.*, 2023, **66**, 3088–3105; (*c*) J. Karges, M. A. Giardini, O. Blacque, B. Woodworth, J. L. Siqueira-Neto and S. M. Cohen, *Chem. Sci.*, 2023, **14**, 711–720.

31 (*a*) L. Panchariya, W. A. Khan, S. Kuila, K. Sonkar, S. Sahoo, A. Ghoshal, A. Kumar, D. K. Verma, A. Hasan, M. A. Khan, N. Jain, A. K. Mohapatra, S. Das, J. K. Thakur, S. Maiti, R. K. Nanda, R. Halder, S. Sunil and A. Arockiasamy, *Chem. Commun.*, 2021, **57**, 10083; (*b*) X. Tao, L. Zhang, L. Du, K. Lu, Z. Zhao, Y. Xie, X. Li, S. Huang, P.-H. Wang, J.-A. Pan, W. Xia, J. Dai and Z.-W. Mao, *J. Inorg. Biochem.*, 2022, **231**, 111777.

32 J. D. Baker, R. L. Uhrich, G. C. Kraemer, J. E. Love and B. C. Kraemer, *PLoS One*, 2021, **16**, e0245962.

33 (*a*) C. Coelho, G. Gallo, C. B. Campos, L. Hardy and M. Würtele, *PLoS One*, 2020, **15**, e0240079; (*b*) J. Chen, Y. Zhang, D. Zeng, B. Zhang, X. Ye, Z. Zeng, X.-K. Zhang, Z. Wang and H. Zhou, *Biochem. Biophys. Res. Commun.*, 2022, **591**, 118–123.

34 D. Graf, N. Farn, J. Klopf, M. Hojjati and U. Schatzschneider, *Metallomics*, 2023, **15**, mfad023.
35 R. Kasprzyk, T. J. Spiewla, M. Smietanski, S. Golojuch, L. Vangeel, S. de Jonghe, D. Jochmans, J. Neyts, J. Kowalska and J. Jemielity, *Antiviral Res.*, 2021, **193**, 105142.
36 C. Abbehausen, *Metallomics*, 2019, **11**, 15–28.
37 (*a*) K. Kluska, M. D. Peris-Díaz, D. Płonka, A. Moysa, M. Dadlez, A. Deniaud, W. Bal and A. Krężel, *Chem. Commun.*, 2020, **56**, 1329–1332; (*b*) K. Kluska, G. Veronesi, A. Deniaud, B. Hajdu, B. Gyurcsik, W. Bal and A. Krężel, *Angew. Chem., Int. Ed.*, 2022, **61**, e202116621; (*c*) G. Park, Z. N. Amaris, M. K. Eiken, K. V. Baumgartner, K. A. Johnston, M. A. Williams, J. G. Markwordt, J. E. Millstone, K. E. Splan and K. E. Wheeler, *Environ. Sci.: Nano*, 2019, **6**, 2367–2378.
38 Q. Zhang, R. Wang, M. Wang, C. Liu, M. Koohi-Moghadam, H. Wang, P.-L. Ho, H. Li and H. Sun, *Proc. Natl. Acad. Sci. U. S. A.*, 2022, **119**, e2119417119.
39 T. Rehm, M. Rothemund, A. Bär, T. Dietel, R. Kempe, H. Kostrhunova, V. Brabec, J. Kasparkova and R. Schobert, *Dalton Trans.*, 2018, **47**, 17367–17381.
40 H. M. J. Wang, C. Y. L. Chen and I. J. B. Lin, *Organometallics*, 1999, **18**, 1216–1223.
41 Y. Han, H. V. Huynh and L. L. Koh, *J. Organomet. Chem.*, 2007, **692**, 3606–3613.
42 X. Ling, N. Schaeffer, S. Roland and M.-P. Pileni, *Langmuir*, 2013, **29**, 12647.
43 H. V. Huynh, T. T. Lam and H. T. T. Luong, *RSC Adv.*, 2018, **8**, 34960–34966.
44 W. Zhu, M. Xu, C. Z. Chen, H. Guo, M. Shen, X. Hu, P. Shinn, C. Klumpp-Thomas, S. G. Michael and W. Zheng, *ACS Pharmacol. Transl. Sci.*, 2020, **3**, 1008–1016.
45 D. Bojkova, P. Reus, L. Panosch, M. Bechtel, T. Rothenburger, J. Kandler, A. Pfeiffer, J. U. Wagner, M. Shumliakivska, S. Dimmeler, R. Olmer, U. Martin, F. Vondran, T. Toptan, F. Rothweiler, R. Zehner, H. Rabenau, K. L. Osman, S. T. Pullan, M. Carroll, R. Stack, S. Ciesek, M. N. Wass, M. Michaelis and J. Cinatl, Identification of novel antiviral drug candidates using an optimized SARS-CoV-2 phenotypic screening platform, *iScience*, 2023, **26**, 105944.